Miner Petrol (2018) 112:111–121
DOI 10.1007/s00710-017-0515-1

ORIGINAL PAPER

Kampelite, $Ba_3Mg_{1.5}Sc_4(PO_4)_6(OH)_3{\cdot}4H_2O$, a new very complex Ba-Sc phosphate mineral from the Kovdor phoscorite-carbonatite complex (Kola Peninsula, Russia)

Victor N. Yakovenchuk[1] · Gregory Yu. Ivanyuk[1] · Yakov A. Pakhomovsky[1] · Taras L. Panikorovskii[1,2] · Sergei N. Britvin[1,2] · Sergey V. Krivovichev[1,2] · Vladimir V. Shilovskikh[3] · Vladimir N. Bocharov[3]

Received: 6 April 2017 / Accepted: 17 May 2017 / Published online: 12 June 2017

Abstract Kampelite, $Ba_3Mg_{1.5}Sc_4(PO_4)_6(OH)_3{\cdot}4H_2O$, is a new Ba-Sc phosphate from the Kovdor phoscorite-carbonatite complex (Kola Peninsula, Russia). It is orthorhombic, *Pnma*, a = 11.256(1), b = 8.512(1), c = 27.707(4) Å, V = 2654.6(3) Å^3 and Z = 4 (from powder diffraction data) or a = 11.2261(9), b = 8.5039(6), c = 27.699(2) Å, V = 2644.3(3) Å^3 (from single-crystal diffraction data). The mineral was found in a void within the calcite-magnetite phoscorite (enriched in hydroxylapatite and Sc-rich baddeleyite) inside the axial zone of the Kovdor phoscorite-carbonatite pipe. Kampelite forms radiated aggregates (up to 1.5 mm in diameter) of platy crystals grown on the surfaces of crystals of quintinite-2*H* in close association with pyrite, bobierrite and quintinite-3*R*. Kampelite is colourless, with a pearly lustre and a white streak. The cleavage is perfect on {001}, the fracture is smooth. Mohs hardness is about 1. In transmitted light, the mineral is colourless without pleochroism or dispersion. Kampelite is biaxial + (pseudouniaxial), $\alpha \approx \beta$ = 1.607(2), γ = 1.612(2) (589 nm), and $2V_{calc}$ = 0°. The calculated and measured densities are 3.28 and 3.07(3) g·cm^{-3}, respectively. The mean chemical composition determined by electron microprobe is: MgO 4.79, Al_2O_3 0.45, P_2O_5 31.66, K_2O 0.34, Sc_2O_3 16.17, Mn_2O_3 1.62, Fe_2O_3 1.38, SrO 3.44, and BaO 29.81 wt%. The H_2O content estimated from the crystal-structure refinement is 7.12 wt%, giving a total of 96.51 wt%. The empirical formula calculated on the basis of P = 6 apfu (atoms per formula unit) is $(Ba_{2.62}Sr_{0.45}K_{0.10}Ca_{0.06})_{\Sigma 3.23}Mg_{1.60}Mn_{0.28}(Sc_{3.15}Fe^{3+}_{0.23}Al_{0.12})_{\Sigma 3.50}(PO_4)_6(OH)_{2.61}{\cdot}4.01H_2O$. The simplified formula is $Ba_3Mg_{1.5}Sc_4(PO_4)_6(OH)_3{\cdot}4H_2O$. The mineral easily dissolves in 10% cold HCl. The strongest X-ray powder-diffraction lines [listed as d in Å (I) (hkl)] are as follows: 15.80(100)(001), 13.86(45)(002), 3.184(18)(223), 3.129(19)(026), 2.756(16)(402), 2.688(24)(10$\underline{10}$). The crystal structure of kampelite was refined to R_1 = 0.092 on the basis of 2620 unique observed reflections. It is based upon complex $[MgBa_2Sc_4(PO_4)_6]$ layers consisting of the Ba-PO_4 zigzag sheet inserted between two Mg-Sc-PO_4 sheets. Raman spectrum of kampelite contains characteristic bands of vibrations of the PO_4, ScO_6 and H_2O groups. Kampelite formed as a result of low-temperature hydrothermal alteration of Sc-bearing baddeleyite, which also produces Sc-rich pyrochlore and juonniite. The structural complexity parameters for kameplite are equal to 5.272 bits/atom and 1244.304 bits/cell, which points out that the mineral is structurally very complex, in agreement with its late-stage hydrothermal origin. The mineral is named in honour of Russian mining engineer Felix Borisovich Kampel' (b. 1935) for his contribution to the development of technologies of mining and processing of complex magnetite-apatite-baddeleyite ores of the Kovdor deposit.

Keywords Kampelite · New mineral · Scandium-barium phosphate · Phoscorite · Kovdor

Editorial handling: N. V. Chukanov

Electronic supplementary material The online version of this article (doi:10.1007/s00710-017-0515-1) contains supplementary material, which is available to authorized users.

✉ Sergey V. Krivovichev
s.krivovichev@spbu.ru

[1] Kola Science Centre, Russian Academy of Sciences, 14 Fersman Street, Apatity 184200, Russia

[2] Department of Crystallography, St. Petersburg State University, 7–9 University Emb, St. Petersburg 199034, Russia

[3] Geo Environmental Centre "Geomodel", St. Petersburg State University, Ul'yanovskaya Str, St. Petersburg 198504, Russia

Introduction

With the inferred resources of 420 t Sc_2O_3, the Kovdor magnetite-apatite-baddeleyite deposit can be considered as a largest source of Sc in Russia (Kalashnikov et al. 2016). Until recently, there were quite a few known minerals containing scandium in appreciable quantities: baddeleyite (on average, 0.08 wt% of Sc_2O_3), pyrochlore-group minerals (0.02 wt%), zirconolite (0.03 wt%), juonniite (12.72 wt%), ilmenite (0.04 wt%), geikielite (0.02 wt%) and pyrophanite (0.23 wt%). Baddeleyite is the major primary concentrator of Sc, and higher Sc content causes more intensive baddeleyite replacement by pyrochlore and/or zirconolite (Ivanyuk et al. 2016).

Juonniite, $CaMgSc(PO_4)_2(OH)\cdot 4H_2O$, is a late-stage hydrothermal mineral that occurs in calcite-incrusted voids and fractures within phoscorites (forsterite-apatite-magnetite-carbonate rock that gradually transforms to carbonatite when carbonate content exceeds 50 modal %) enriched in Sc-bearing baddeleyite, pyrochlore and zirconolite, as well as within veins of dolomite carbonatite that cut through these phoscorites (Liferovich et al. 1997; Ivanyuk et al. 2002). Juonniite formed as a result of hydrothermal alteration of carbonate-rich phoscorites or carbonatites, initially containing Sc-Nb-rich baddeleyite and hydroxylapatite (Kalashnikov et al. 2016). Enrichment of hydroxylapatite of the pipe axial zone by barium (Ivanyuk et al. 2016) results in the presence in carbonate-rich phoscorite of numerous Ba minerals such as baryte, barytocalcite, henrymeyerite, rimkorolgite, krasnovite, gorceixite, norsethite, and kampelite, which is a new mineral of Sc and Ba found as two small spherulites in a void within calcite-magnetite phoscorite enriched in Sc-bearing baddeleyite, pyrochlore and zirconolite as well as in Ba-bearing hydroxylapatite. The mineral is named in honour of Russian mining engineer Felix Borisovich Kampel' (born 1935) who was Technical Director of the Kovdor Mining and Dressing Plant 1991–2003. The name honours F.B. Kampel's contribution to the development of technologies of mining and processing of complex magnetite-apatite-baddeleyite ores of the Kovdor deposit (Kampel' et al. 1982, 1997; Lyakhov et al. 1997; Lokshin et al. 2002). The new mineral and its name were approved by the Commission on New Minerals, Nomenclature and Classification of the International Mineralogical Association (IMA CNMNC; proposal 2016–084). The holotype specimen is deposited in the collections of the Mineralogical Museum of St. Petersburg State University, Russia, under catalogue number 1/19660.

Occurrence

The Kovdor massif of peridotites, foidolites, melilitolites, phoscorites, carbonatites and related metasomatic rocks (diopsidites, phlogopitites, skarn-like rocks, and fenites) is situated in the southwest part of the Murmansk region, Russia (N 67°33′, E 30°31′). It is of a central-type, polyphase volcano-plutonic complex (Fig. 1a) intruded through the Archean biotite and hornblende-biotite (granite-)gneiss about 400 million years ago (Rodionov et al. 2012; Mikhailova et al. 2016). The stock of the earliest peridotite (up to 8 km in initial diameter) is coated by the ring intrusion of foidolite–melilitolite (up to 1 km thick) that causes intensive metasomatic alteration of both outer granite-gneiss and internal peridotite forming diopsidites, phlogopitites, melilite-, monticellite-, vesuvianite- and andradite-rich skarn-like rocks (after peridotite), fenitized gneisses and fenites (after granite-gneisses). The main rocks of the massif as well as the host granite-gneisses are penetrated by numerous veins and dykes of nepheline and cancrinite syenites, ijolites, phonolites, alnoites, shonkinites, calcite- and dolomite-calcite carbonatites (Ivanyuk et al. 2002; Mikhailova et al. 2016).

The western contact of peridotite and foidolite intrusions is intruded by a vertical concentrically zoned pipe of phoscorites and phoscorite-related carbonatites, with later stockworks of vein calcite and dolomitic carbonatites (Fig. 1b). The pipe zonality can be described by the following sequence of rocks: primary (apatite)-forsterite rich phoscorites of the marginal zone – magnetite-rich carbonate-poor phoscorites of the intermediate zone – carbonate-rich phoscorites and phoscorite-related carbonatites of the axial zone – vein calcite carbonatite – vein dolomite carbonatite and magnetite-dolomite-serpentine rock (Mikhailova et al. 2016; Ivanyuk et al. 2016). Within this sequence, the Sc content in baddeleyite increases from <0.02 to 0.3 wt%, whereas the Ba content in hydroxylapatite grows from <0.05 to 1.7 wt%. The type locality of kampelite is situated in the carbonate-magnetite-rich phoscorite of the ore-pipe axial zone (Fig. 1c).

The mineral was found in the calcite-magnetite phoscorite outcropped on the bottom of the Iron open pit at the horizon −100 m (Fig. 1a). The primary minerals include forsterite and hydroxylapatite (up to 5 modal % of each mineral) that form granular (up to 1 mm in diameter) segregations resorbed by later magnetite and carbonates. Magnetite (up to 84 modal %) forms irregularly shaped metacrysts (up to 20 cm in diameter) that get well-shaped mirror-like faces on the contact with later calcite nests (up to 15 cm in diameter). Magnetite grains always contain (oxy)exsolution inclusions of ilmenite–geikielite (earlier) and spinel (later), and calcite nests always include veinlets and lenses of dolomite (≤10 modal %).

Other accessory minerals are: ScNb-rich baddeleyite, partially replaced by a pyrochlore-group mineral, microlite and zirconolite, strontianite, barytocalcite, ancylite-(Ce), pyrrhotite with exsolution lamellae of cobaltpentlandite, pyrite, sphalerite, chalcopyrite, galena, valleriite, thorianite, monazite-(Ce), rhabdophane-(Ce), magnesite, quintinite, witherite, norsethite, burbankite, shortite, eitelite, nyerereite,

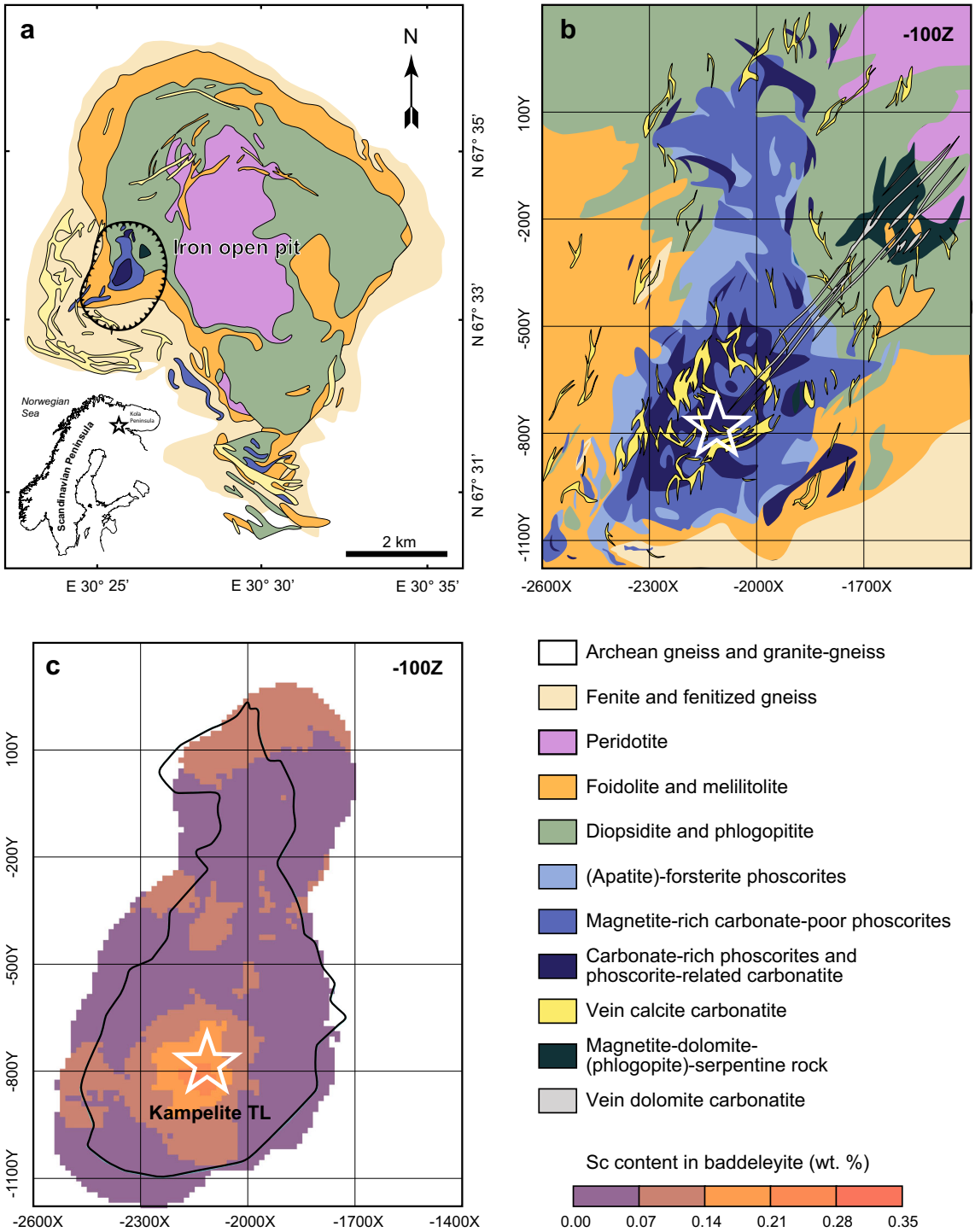

Fig. 1 **a** Geological map of the Kovdor massif (after Mikhailova et al. 2016). **b** Geological map of the phoscorite-carbonatite pipe (after Ivanyuk et al. 2016). **c** Distribution of Sc in baddeleyite at the −100 m horizon. The position of the kampelite type locality (TL) is marked with a white star

and northupite. Sometimes, the rock is penetrated by monomineralic veinlets of kovdorskite (up to 10 cm thick) and quintinite-1*M* (up to 4 cm thick). In open voids (up to 8 cm in diameter) incrusted by brilliant crystals of magnetite (up to 8 cm in diameter) and calcite (up to 2 cm long), there are well-shaped tabular or pyramidal crystals of quintinite-2*H*, 3*R* and 1*M*, radiated aggregates of bakhchisaraitsevite, bobierrite, juonniite, and kampelite and crystals of magnesite, dolomite and pyrite (Ivanyuk et al. 2002; Mikhailova et al. 2016).

Spherulites of kampelite (up to 1.5 mm in diameter, Fig. 2a) grow on the surfaces of dark-orange pyramidal crystals of quintinite-2*H* (up to 5 mm long) in close association with cubic crystals of pyrite (up to 1 mm in diameter), grey spherulites of bobierrite (up to 2 cm in diameter) and yellow crystals of

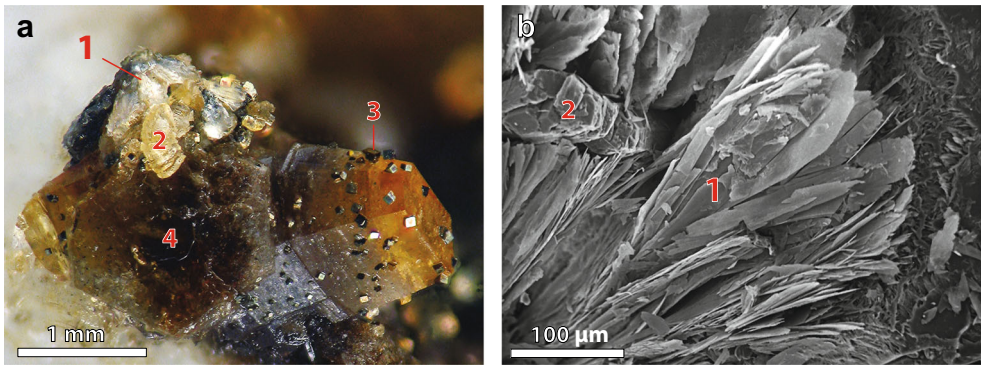

Fig. 2 White-light photograph (**a**) and secondary-electrons image (**b**) of radiated aggregates of kampelite (**1**) intergrown with quintinite-3*R* (**2**) and pyrite (**3**), on crystals of quintinite-2*H* (**4**)

quintinite-3*R* (up to 1 mm long). In turn, crystals of quintinite-2*H* grow on calcite and magnetite crystals, encrusting walls of the voids (about 5 cm in diameter) within the calcite-magnetite phoscorite.

Mineral description and properties

General description

Kampelite forms radiated aggregates of split plates (up to 700 μm long and 30 μm thick, Fig. 2b) elongated along [010] and flattened on {010}. Radiated aggregates of kampelite are friable and brittle, while its separated plates are flexible and have a smooth fracture. The cleavage is perfect on {001}. Neither twinning nor parting was observed. The Mohs hardness is about 1 (the mineral does not scratch a transparent hypsum plate). The specific gravity, determined by the float-sink method in Clerici solution, is 3.07(3) g/cm^3, and the calculated density is 3.28 g/cm^3 (using the empirical formula and single-crystal unit-cell parameters). The observed difference between the measured and calculated density values is most probably caused by admixtures of mineral phases with lower density.

Macroscopically, radiated aggregates of kampelite are silvery-white, and its separated plates are colourless with a pearly lustre. The aggregates are translucent, and separate plates are transparent, with a white streak. Kampelite is biaxial positive (pseudouniaxial), with refractive indices $\alpha \approx \beta = 1.607 \pm 0.002$ and $\gamma = 1.612 \pm 0.002$ at 589 nm. In transmitted light, the mineral is colorless, without pleochroism and dispersion. The mineral is non-fluorescent. A Gladstone-Dale calculation provides a compatibility index of 0.046 (with the empirical formula and single-crystal XRD data), which is regarded as good (Mandarino 1981).

Chemical composition

The chemical compositions of kampelite were determined by wavelength-dispersive spectrometry using a Cameca MS-46 electron probe micro-analyzer operated at 20 kV, 20–30 nA, with a 10 μm beam diameter. The calibrant materials used (with the respective elements in brackets) were: pyrope (Mg and Al), fluorapatite (P), wadeite (K), diopside (Ca), thortveitite (Sc), hematite (Fe), celestine (Sr), barite (Ba) and synthetic $MnCO_3$ (Mn). The mineral is unstable under the electron beam and loses a fraction of its water after few seconds of analyzing. In order to obtain reliable analytical data, the electron beam was defocused and moved during the analyses. In addition, the mineral loses some water in a vacuum before the analyzing. Taking this into account, the H_2O content in kampelite was estimated on the basis of crystal-structure refinement.

Table 1 provides average analytical results for three different kampelite plates. The mean chemical composition of kampelite corresponds to the following empirical formula (calculated on the basis of $P = 6$): $(Ba_{2.62}Sr_{0.45}K_{0.10}Ca_{0.06})_{\Sigma 3.23}Mg_{1.60}Mn_{0.28}(Sc_{3.15}Fe^{3+}_{0.23}Al_{0.12})_{\Sigma 3.50}(PO_4)_6(OH)_{2.61}\cdot 4.01H_2O$. The Sc content decreases linearly with the increasing amount of Mg and K (Fig. 3), following the charge-compensating scheme $Sc^{3+} + \square \leftrightarrow K^+ + Mg^{2+}$. This substitution results in the permanent excess of cations in the Ba and Mg sites and the corresponding deficit of cations in the Sc site (see below). Taking this into account, the simplified formulae of kampelite can be written as $Ba_{3+0.5x}Mg_{1+x}Mn_{0-0.5}Sc_{4-x}(PO_4)_6(OH)_3\cdot 4H_2O$ or $Ba_3Mg_{1.5}Sc_4(PO_4)_6(OH)_3\cdot 4H_2O$ (Fig. 3).

Raman spectroscopy

Raman spectrum of kampelite (Fig. 4) was obtained using a Horiba Jobin-Yvon LabRam HR 800 spectrometer (wavelength 514 nm). Assignments of absorption bands in the Raman spectrum of kampelite have been made by its comparison with the spectra of other phosphates and carbonates, including hureaulite and sampleite (Frost et al., 2007, 2013). The most intensive band at 975 as well as the shoulder at 932 cm^{-1} corresponds to the symmetric stretching vibration of the phosphate anion, PO_4^{3-}. Another intensive band at 1092 cm^{-1} can be assigned to the ν_3 antisymmetric stretching vibrations of the PO_4^{3-} group. Other Raman bands in the

Table 1 Chemical compositions and calculated cation contents of kampelite

Component	1	2	3	Mean	SD*	Ideal
Oxide contents measured (wt%):						
MgO	5.63	4.22	4.53	4.79	0.74	4.61
Al_2O_3	b.d.l.	1.36	b.d.l.	0.45	0.79	
P_2O_5	33.91	30.18	30.90	31.66	1.98	32.45
K_2O	0.39	0.30	0.32	0.34	0.05	
CaO	0.26	0.29	0.21	0.25	0.04	
Sc_2O_3	17.17	15.54	15.81	16.17	0.87	21.02
MnO	1.46	1.50	1.41	1.46	0.05	
FeO	1.13	1.24	1.36	1.24	0.12	
SrO	4.17	3.38	2.76	3.44	0.71	
BaO	31.54	27.25	30.65	29.81	2.26	35.06
H_2O_{calc}**				7.12		6.87
Total	95.66	85.26	87.95	97.03		100.00
*Cation contents (apfu)****:						
Ba	2.58	2.51	2.76	2.62	0.13	3
Sr	0.51	0.46	0.37	0.45	0.07	
K	0.10	0.09	0.09	0.10	0.01	
Ca	0.06	0.07	0.06	0.06	0.01	
Mg	1.75	1.48	1.55	1.60	0.14	1.5
Mn	0.26	0.30	0.27	0.28	0.02	
Sc	3.13	3.18	3.16	3.15	0.03	4
Al	0.00	0.38	0.00	0.12	0.22	
Fe^{3+}	0.20	0.24	0.26	0.23	0.03	
P	6.00	6.00	6.00	6.00	0.00	6
H				10.63		11

b.d.l. = below the EPMA detection limit

*SD = standard deviation

**Calculated from the structural data

***Cations per formula unit were calculated based on 6 P atoms per formula unit

range 450–850 cm^{-1} can be attributed to the symmetric ν_2 and antisymmetric bending ν_4 vibrations of the PO_4^{3-} groups. The H_2O bending band is observed at around 1604 cm^{-1}. The bands at 297 and 402 cm^{-1} correspond to the stretching and bending modes of the Sc–O bonds and O-Sc-O angles, respectively. The bands observed at 77 and 173 cm^{-1} can be related to the Ba–O ν_1 or external lattice vibrations. Assignment of all observed bands is given in Table 2.

Crystal structure

Single-crystal X-ray diffraction study was performed using Bruker Kappa APEX DUO diffractometer equipped with the IμS microfocus source (beam size of 0.11 mm) and a CCD area detector operated at 45 kV and 0.6 mA. Due to the small size and flexibility of the crystals of kampelite (Fig. 2b), collection of reliable X-ray diffraction data was rather difficult.

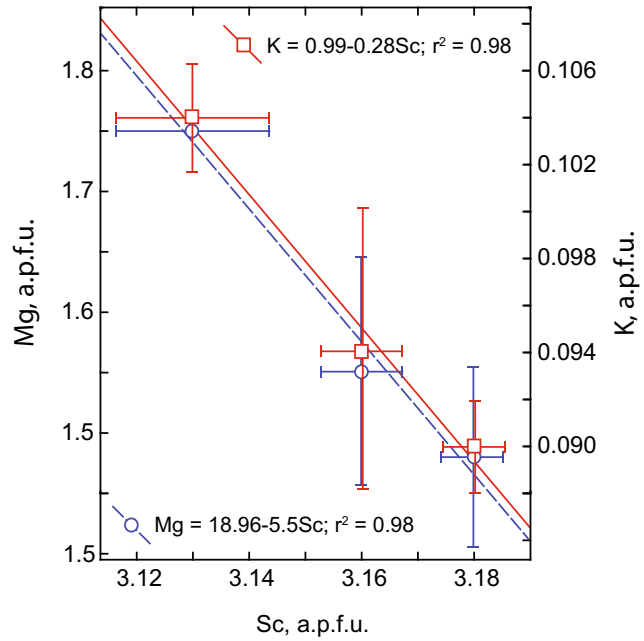

Fig. 3 Relation between the Sc, Mg and K contents as obtained for three kampelite plates. Bars indicate standard deviations

Very few reflections have been recorded using normally employed Mo*K*α radiation (λ = 0.71073 Å), which did not allow to obtain any reasonable dataset. The change to the Cu*K*α radiation (λ = 1.54184 Å) made it possible to collect enough diffraction data to reveal basic features of atomic arrangement in the crystal structure of kampelite. Still, the quality of the structure refinement was far from perfect, which is reflected in the high values of *R* indices (see below). The intensity data were reduced and corrected for Lorentz, polarization and background effects. A multi-scan absorption-correction was applied by the Bruker software APEX2 (Bruker-AXS 2014). The crystal structure was solved by direct methods with the ShelX program package (Sheldrick 2008) and refined to $R_1 = 0.092$ ($R_{int} = 0.0830$) for 2620 independent reflections with $F_o > 4\sigma(F_o)$. The occupancies of the cation sites have been determined on the basis of experimental site-scattering factors compared with the empirical chemical composition. Hydrogen sites could not be located. Inspection of difference Fourier electron-density maps revealed the presence of a relatively high peak (Q), which corresponds to the position of the Ba atom of the layer shifted along the *a* axis. This kind of residual peaks usually appears in the layered structures with pronounced stacking faults (Krivovichev et al. 2003). Crystal data, data collection information and structure refinement details are given in Table 3, atom coordinates and selected interatomic distances are in Tables 4 and 5, respectively. Anisotropic displacement parameters and other details of structure refinement are deposited as a supplementary CIF (Crystallographic Information File).

The crystal structure of kampelite contains two Sc sites, each coordinated by six O atoms with the average < Sc-O > bond-

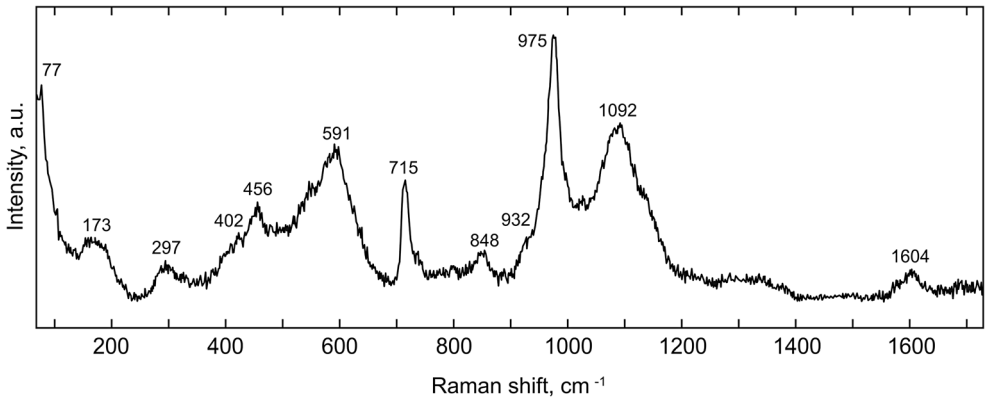

Fig. 4 Raman spectrum of kampelite

lengths equal to 2.120 and 2.113 Å for Sc1 and Sc2, respectively (Fig. 5b). These values can be compared to the average < Sc-O > distances in ScO6 octahedra in other Sc phosphates, e.g. kolbeckite, $ScPO_4 \cdot 2H_2O$ (2.080 Å: Yang et al. 2007), $KSc(HPO_4)_2$ (2.092 Å: Menezes et al. 2009), $Li_2Sc[(PO_4)(HPO_4)]$ (2.095 Å: Menezes et al. 2008). Both Sc sites have additional admixtures of Fe and Al (Table 4). There are two Ba sites in the crystal structure of kampelite, Ba1 and Ba2, coordinated by nine and eight O atoms, respectively (Fig. 5b). The Ba1 site has an admixture of Sr and its full occupancy is 100%, whereas Ba2 site is half-occupied (the distance between two symmetry-related Ba2 sites is 2.533 Å) and has the occupancy $Ba_{0.42}(H_2O)_{0.08}$.

The structure of kampelite contains six independent P sites tetrahedrally coordinated by four O atoms each. The average < P-O > bond lengths vary from 1.516 to 1.531 Å, which agrees well with the average P-O distance of 1.537 Å given for phosphates by Huminicki and Hawthorne (2002).

There are two partially occupied Mg sites in kampelite, Mg1 and Mg2, coordinated by six and seven O atoms, respectively. The refined site-occupation factors are 0.57 and 0.79, respectively. The structure also contains two low-occupied Mn sites that form dimers of face-sharing MnO_6 octahedra (Fig. 5b). However, the occupancies of the Mn sites are rather low (0.18 and 0.24 for Mn1 and Mn2, respectively), which means that the dimers do not exist in the real structure (the Mn1-Mn2 distances across the shared face is 2.217 Å).

Considering cation sites with more than 50% occupancy, the crystal structure of kampelite can be considered as based on the $[MgBa_2Sc_4(OH)_2(PO_4)_6]^{2-}$ anionic layers parallel to the (001) plane and separated by disordered interlayer species (Fig. 5a). Each layer has the Ba phosphate sheet sandwiched between two Mg-Sc-PO_4 sheets. The Ba-phosphate sheets (Fig. 6a) are built by columns of edge-sharing $Ba1O_9$ polyhedra running along [010] and interlinked by the $P3O_4$ and $P4O_4$ tetrahedra. The Mg-Sc-PO_4 sheet (Fig. 6b) is based upon chains formed by dimers of edge-sharing ScO_6 octahedra, which are further

Table 2 Raman bands in the kampelfelite spectrum and their interpretation

Raman shift, cm^{-1}	Assignment	Type
1604	H_2O	ν_2
932(sh), 975(s)	PO_4	ν_1
1092(s)	PO_4	ν_3
456	PO_4	ν_2
591	PO_4	ν_4
715(s)	Sc-OH bending vibrations	ν_2, ν_4
297, 402	ScO_6	ν_1, ν_2
77, 173	Ba-O and external lattice vibrations	ν_1

sh shoulder, *s* strong intensity

Table 3 Crystallographic data and refinement parameters for kampelite

Temperature/K	293(2)
Crystal system	orthorhombic
Space group	*Pnma*
a (Å)	11.2261(9)
b (Å)	8.5039(6)
c (Å)	27.699(2)
V ($Å^3$)	2644.3(3)
Z	4
ρ_{calc} (g/cm^3)	3.370
M (mm^{-1})	49.111
F(000)	2483.0
Crystal size (mm^3)	0.11 × 0.08 × 0.001
Radiation	Cu*K*α (λ = 1.54184)
Θ range for data collection (°)	3.191 to 69.787
Index ranges	$-13 \le h \le 12$, $-10 \le k \le 10$, $-19 \le l \le 33$
Reflections collected	10,829
Independent reflections	2617 [R_{int} = 0.083, R_{sigma} = 0.051]
Data/restraints/parameters	2617/78/273
Goodness-of-fit on F^2	1.081
Final *R* indexes [$I \ge 2\sigma(I)$]	R_1 = 0.092, wR_2 = 0.243
Final *R* indexes [all data]	R_1 = 0.117, wR_2 = 0.269
Largest diff. Peak/hole / $e^-Å^{-3}$	4.06/−2.68

Table 4 Atomic coordinates, occupancies and equivalent isotropic displacement parameters U_{eq} for kampelite

Atom	Occupancy	*x*	*y*	*z*	U_{iso}
Ba1	$Ba_{0.83}Sr_{0.17}$	0.10456(7)	0.00071(9)	0.30234(3)	0.0169(5)
Ba2	$Ba_{0.42}(H_2O)_{0.08}$	0.4070(3)	0.0140(3)	0.47447(11)	0.0397(11)
Sc1	$Sc_{0.81}Fe_{0.10}Al_{0.05}$	0.4466(2)	0.0536(3)	0.33164(9)	0.0106(9)
Sc2	$Sc_{0.82}Fe_{0.10}Al_{0.05}$	−0.2381(2)	−0.0530(3)	0.33405(9)	0.0109(9)
Mg1	$Mg_{0.57}$	0.2950(15)	¾	0.3798(7)	0.071(10)
Mg2	$Mg_{0.79}$	−0.0891(14)	¼	0.3835(8)	0.101(11)
Mn1	$Mn_{0.18}$	−0.1058(17)	¾	0.4994(7)	0.024(7)
Mn2	$Mn_{0.24}$	0.3028(16)	¼	0.4951(6)	0.032(5)
P1	P	0.5583(4)	¾	0.39845(17)	0.0117(10)
P2	P	0.2247(4)	¼	0.38639(18)	0.0143(11)
P3	P	0.3724(4)	¾	0.26149(17)	0.0095(10)
P4	P	-0.1636(4)	¼	0.26315(15)	0.0079(10)
P5	P	0.6447(4)	¼	0.40006(17)	0.0130(11)
P6	P	-0.0111(5)	¾	0.38553(18)	0.0160(11)
O1	O	-0.0021(11)	¾	0.2576(4)	0.010(2)
O2	O	0.3431(9)	−0.1051(11)	0.2914(3)	0.015(2)
O3	O	0.1096(12)	¾	0.3619(5)	0.021(3)
O4	O	-0.0780(9)	−0.1020(11)	0.3691(3)	0.016(2)
O5	O	-0.1349(8)	0.1037(11)	0.2938(3)	0.013(2)
O6	O	0.2101(13)	¼	0.2549(5)	0.017(3)
O7	O	0.1023(13)	¼	0.3640(6)	0.026(4)
O8	O	-0.2128(11)	¾	0.2832(4)	0.012(3)
O9	O	0.4241(12)	¼	0.2795(5)	0.014(3)
O10	OH	0.6087(10)	−0.0019(13)	0.2975(4)	0.024(3)
O11	O	0.4866(9)	−0.1033(11)	0.3853(3)	0.017(2)
O12	O	0.5333(12)	¼	0.3673(4)	0.010(2)
O13	O	0.6762(12)	¾	0.3699(5)	0.015(3)
O14	O	0.5821(14)	¾	0.4504(5)	0.021(3)
O15	O	0.7210(9)	0.1068(12)	0.3887(4)	0.020(2)
O16	O	0.6053(18)	¼	0.4527(6)	0.039(5)
O17	O	0.222(2)	¼	0.4415(7)	0.047(5)
O18	O	0.2903(9)	0.1043(11)	0.3685(4)	0.019(2)
O19	O	0.0010(16)	¾	0.4398(6)	0.032(4)
O20A	$(OH)_{0.50}$	0.042(5)	¾	0.5401(17)	0.09(3)
O20B	$(H_2O)_{0.50}$	-0.004(3)	−0.082(9)	0.5413(15)	0.14(3)
O21	H_2O	0.253(2)	¾	0.4582(13)	0.093(10)
O22	$(H_2O)_{0.84}(OH)_{0.16}$	0.7965(12)	−0.0537(17)	0.4726(5)	0.040(3)
Q*	-	0.1961(11)	−0.0030(13)	0.1973(3)	0.006(4)

*Ghost electron-density peak due to stacking faults

linked by sharing common corners to form an octahedral chain extended along the **b** axis. The chains are surrounded by the PO_4 tetrahedra centered by P1, P2, P5 and P6 atoms. The mixed octahedral-tetrahedral chains are linked by MgO_n polyhedra (n = 6, 7) to complement the formation of the sheet.

The $[MgBa_2Sc_4(OH)_2(PO_4)_6]^{2-}$ layers are separated by an interlayer space filled by low-occupied Ba^{2+}, Mn^{2+}, $(OH)^-$, and H_2O sites. The high degree of disorder in the interlayer and the low quality of structure refinement do not allow to determine precise short-range order configurations, so the site assignments given in Table 4 should be considered as tentative hypothesis rather than definite determination.

The crystal-chemical formula of kampelite determined on the basis of the structure refinement is $(Ba_{2.50}Sr_{0.34})_{\Sigma 2.84}$ $Mg_{1.36}Mn_{0.42}(Sc_{3.26}Fe^{3+}_{0.40}\ Al_{0.20})_{\Sigma 3.86}$ $(PO_4)_6(OH)_{2.82}$ $(H_2O)_{4.00}$, which is in good agreement with its empirical

Table 5 Selected interatomic distances (Å) in the crystal structure of kampelite

Ba1-O1	2.741(8)	Sc1-O2	2.101(9)	P4-O5	1.541(9) 2×
Ba1-O2	2.842(10)	Sc1-O9	2.221(9)	P4-O6	1.503(15)
Ba1-O3	2.696(9)	Sc1-O10	2.105(11)	P4-O9	1.538(14)
Ba1-O4	2.894(10)	Sc1-O11	2.047(10)	<P4-O>	1.531
Ba1-O5	2.837(10)	Sc1-O12	2.171(8)		
Ba1-O6	2.762(9)	Sc1-O18	2.075(10)	P5-O12	1.546(13)
Ba1-O7	2.723(11)	<Sc1-O>	2.120	P5-O15	1.521(10) 2×
Ba1-O10	2.765(10)			P5-O16	1.524(18)
Ba1-O19	2.913(11)	Sc2-O4	2.084(10)	<P5-O>	1.528
<Ba1-O>	2.797	Sc2-O5	2.088(10)		
		Sc2-O8	2.206(8)	P6-O3	1.505(15)
Ba2-O11	2.810(10)	Sc2-O10	2.043(11)	P6-O4	1.535(9) 2×
Ba2-O14	2.893(11)	Sc2-O13	2.172(9)	P6-O19	1.510(17)
Ba2-O14	3.058(11)	Sc2-O15	2.086(10)	<P6-O>	1.521
Ba2-O16	3.057(15)	<Sc2-O>	2.113		
Ba2-O16	3.021(12)			Mg1-O3	2.14(2)
Ba2-O17	3.032(19)	P1-O11	1.529(9) 2×	Mg1-O11	2.491(18) 2×
Ba2-O21	2.872(17)	P1-O13	1.542(14)	Mg1-O21	2.22(4)
Ba2-O22	2.735(14)	P1-O14	1.464(15)	Mg1-O2	2.795(19) 2×
<Ba2-O>	2.935	<P1-O>	1.516	<Mg1-O>	2.489
Mn1-O19	2.04(3)	P2-O7	1.507(16)	Mg2-O7	2.22(2)
Mn1-O17	2.09(3)	P2-O17	1.528(18)	Mg2-O15	2.459(17) 2×
Mn1-O22	2.131(18) 2×	P2-O18	1.524(9) 2×	Mg2-O20A	2.18(6)
Mn1-O20B	2.17(6) 2×	<P2-O>	1.521	Mg2-O20B	2.73(5) 2×
<Mn1-O>	2.122			Mg2-O5	2.83(2) 2×
		P3-O1	1.505(13)	<Mg2-O>	2.555
Mn2-O17	1.74(3)	P3-O2	1.521(9) 2×		
Mn2-O14	1.99(2)	P3-O8	1.565(12)		
Mn2-O22	2.197(18) 2×	<P3-O>	1.528		
Mn2-Ba2	2.392(10) 2×				
<Mn2-O>	2.151				

formula, $(Ba_{2.62}Sr_{0.45}K_{0.10}Ca_{0.06})_{\Sigma 3.23}Mg_{1.60}Mn_{0.28}(Sc_{3.15}Fe^{3+}_{0.23}Al_{0.12})_{\Sigma 3.50}(PO_4)_6(OH)_{2.61}\ (H_2O)_{4.01}$.

Powder X-ray diffraction pattern (Table 6) was obtained using a Rigaku R-AXIS RAPID II diffractometer equipped with a cylindrical image plate detector using Debye-Scherrer geometry (d = 127.4 mm; Co$K\alpha$ radiation). The data were integrated using the software package Osc2Tab/SQRay (Britvin et al. 2017). The unit-cell parameters refined from the powder data are as follows: *Pnma*, a = 11.256(1) Å, b = 8.512(1) Å, c = 27.707(4) Å, V = 2644.3(3) Å^3 and Z = 4, which are in good agreement with the single-crystal data (Table 3).

Discussion

Processes of alteration and self-cleaning of primary minerals from chemical impurities were very intense at the late stages of the formation of the Kovdor phoscorite-carbonatite pipe (Mikhailova et al. 2016; Ivanyuk et al. 2002, 2016). For example, the exsolution of Mg-Al-rich titanomagnetite produces ilmenite–geikielite, spinel, baddeleyite and then quintinite (Ivanyuk et al. 2002, 2016; Kalashnikov et al. 2016), the exsolution of Ni-Co-rich pyrrhotite results in the formation of pentlandite and cobaltpentlandite followed by pakhomovskyite and gladiusite (Yakovenchuk et al. 2006). The alteration of baddeleyite results in the crystallization of zirconolite, pyrochlore, zircon followed by juonniite and kampelite (Ivanyuk et al. 2002, 2016; Kalashnikov et al. 2016).

Both kampelite and juonniite have been found in the calcite-magnetite phoscorite of the axial zone of the phoscorite-carbonatite pipe. In this rock, baddeleyite is sufficiently enriched in Sc and Nb because of the $2Zr^{4+} \leftrightarrow Sc^{3+}Nb^{5+}$ substitution, whereas hydroxylapatite is comparatively enriched in Ba due to the Ca ↔ (Sr, Ba) substitution (Ivanyuk et al. 2002,

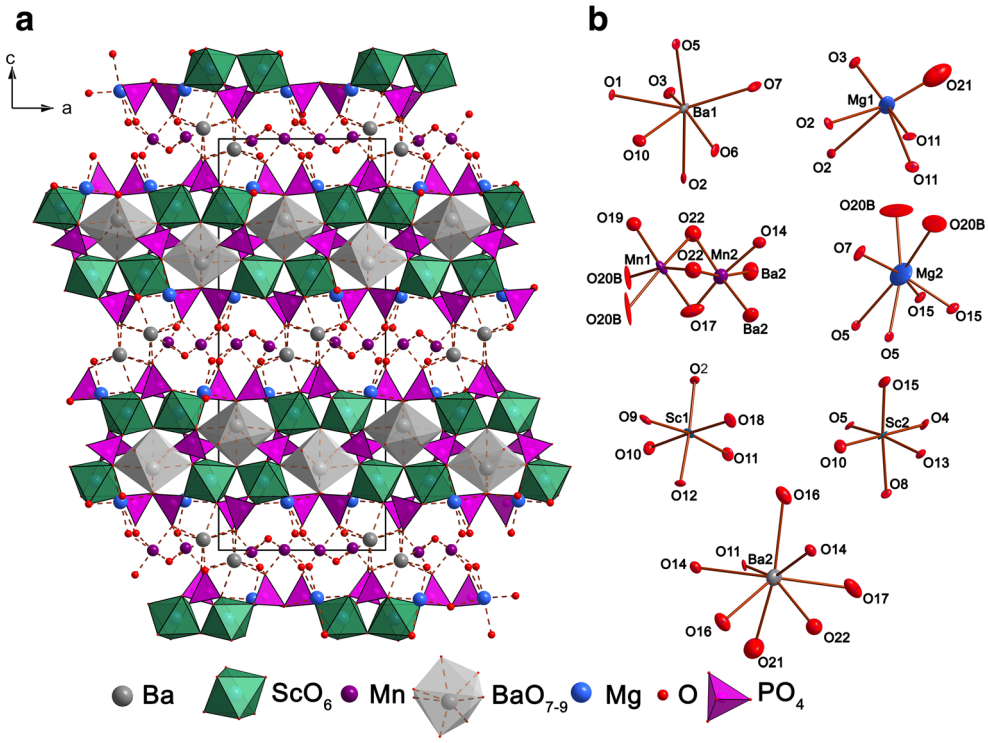

Fig. 5 The crystal structure of kampelite projected along [010] (**a**) and the coordination of Ba, Mg, Mn and Sc (**b**). Displacement ellipsoids are drawn at the 50% probability level

2016). Partial dissolution of rock-forming hydroxylapatite by late-stage fluorine-bearing hydrothermal solutions causes the release of Ba followed by the chemical reaction of Ba-rich solutions with ScNb-rich baddeleyite, which produces Ba-rich (up to 21 wt% BaO) and Sc-poor pyrochlore (Kalashnikov et al. 2016). The residual solution becomes enriched also in Sc, with the consequent precipitation of Sc-(Ba) phosphates:

$$12\mathrm{Bdy}' + 6\mathrm{Dol} + 4\mathrm{Ap} + 25\mathrm{H_2O} + 2\mathrm{CO_2} \rightarrow 6\mathrm{Jnn} + 3\mathrm{Pcl} + 14\mathrm{Cal} \quad (1)$$

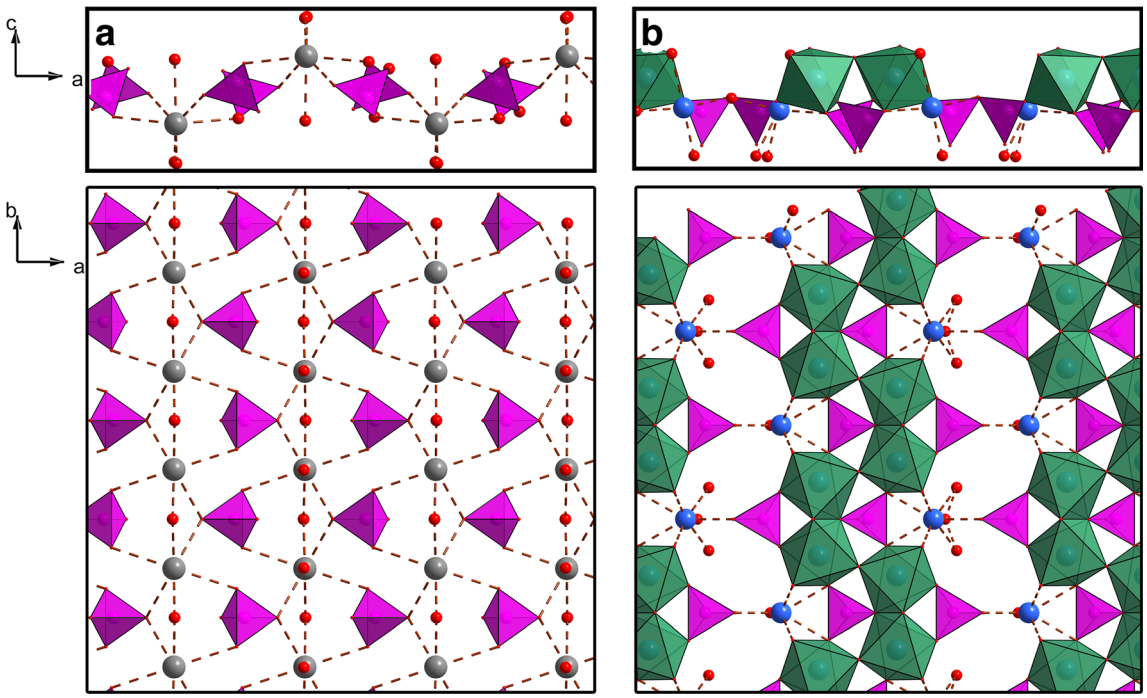

Fig. 6 The topology of the Ba phosphate (**a**) and Mg-Sc-phosphate (**b**) layers in the crystal structure of kampelite

Table 6 X-ray powder diffraction data for kampelite

I_{meas}	$d_{meas,}$Å	$d_{calc,}$Å	*hkl*
100	**15.80**	**15.78**	**001**
45	**13.86**	**13.84**	**002**
10	10.49	10.41	101
6	7.17	7.13	103
3	6.58	6.59	111
2	5.505	5.510	201
9	4.620	4.626	211
3	3.616	3.618	302
3	3.443	3.451	124
4	3.366	3.330	312
11	**3.292**	**3.290**	**216**
18	**3.184**	**3.185**	**223**
19	**3.129**	**3.128**	**026**
14	**3.022**	**3.024**	**217**
5	2.911	2.909	306
3	2.810	2.811	400
16	**2.756**	**2.755**	**402**
24	**2.688**	**2.688**	**1 0 10**
3	2.606	2.606	324
3	2.402	2.402	326
2	2.343	2.346	420
9	2.309	2.310	416
9	2.278	2.279	229
1	2.218	2.218	2 1 11
6	2.184	2.184	1 1 12
4	2.129	2.128	040
1	2.035	2.0344	044
6	1.9875	1.9855	241
3	1.9435	1.9441	523
2	1.8729	1.8732	245
2	1.7902	1.7899	148
10	1.7778	1.7781	247
3	1.7133	1.7133	3 1 14
4	1.6930	1.6938	607
1	1.6797	1.6797	535
1	1.6713	1.6712	152
1	1.5649	1.5650	704
2	1.4529	1.4535	5 2 13
2	1.4292	1.4292	726
2	1.4064	1.4067	640

The eight strongest lines are highlighted bold

$$16\mathrm{Bdy}' + 3\mathrm{Dol} + 4\mathrm{Ap} + 9\mathrm{H_2O} + 9\mathrm{CO_2} + 5\mathrm{O_2} + 6\mathrm{Ba^{2+}} \rightarrow 2\mathrm{Kam} + 4\mathrm{Pcl} + 15\mathrm{Cal} \quad (2)$$

where Ap = hydroxylapatite; Bdy' = Sc-Nb end member of baddeleyite, $Sc_{0.5}Nb_{0.5}O_2$; Cal = calcite, Dol = dolomite; Jnn = juonniite; Kam = kampelite, Pcl = pyrochlore, $Ca_2Nb_2O_7$. Thus, kampelite is a typical secondary mineral crystallized due to the alteration of ScNb-rich baddeleyite by Ba-rich hydrothermal solutions.

The average temperature of the calcite-dolomite pair crystallization in this rock is 440 ± 70 °C (120 samples estimated with the geothermometer of Anovitz and Essene (1987)), whereas the average temperature of titanomagnetite oxy-exsolution is 310 ± 30 °C (21 samples estimated with the geothermometer of Ghiorso and Evans (2008)). Exsolution of residual Mg-Al rich magnetite into impurity-poor magnetite, spinel and quintinite-2*H* occurred at temperatures 300–200 °C, and the crystallization of kampelite and quintinite-3*R* at temperature ≤ 100 °C is quite comparable with the temperature of precipitation of cattiite, $Mg_3(PO_4)_2{\cdot}22H_2O$, estimated as 20 °C (Britvin et al., 2002).

The high complexity of the crystal structure of kampelite manifested in the large number of atom sites as well as in relatively large *c* parameter (27.699 Å) is typical for late-stage secondary minerals formed at low-temperature conditions (Krivovichev 2013). Calculation of structural complexity parameters for kampelite was done using information-based complexity measures developed by Krivovichev (2012, 2014). Since no H atoms could be located, the procedure of H-correction was applied by introducing 'dummy' H sites into the structure model (see (Pankova et al. 2017) for more details). Calculations performed by means of the TOPOS software (Blatov et al. 2014) provided the structural complexity values of 5.272 bits/atom and 1244.304 bits/cell, which points out that kampelite belongs to the group of very complex structures according to the classification scheme by Krivovichev (2013, 2014). The same applies also to juonniite, $CaMgSc(PO_4)_2(OH){\cdot}4H_2O$, which was described by Liferovich et al. (1997) as a Sc analogue of overite, $CaMgAl(PO_4)_2(OH){\cdot}4H_2O$ (Moore 1974). The crystal structure of juonniite has not been reported in the literature, and the structure data for overite (Moore and Araki 1977; complemented by the H-correction) were used to calculate its complexity parameters that are equal to 4.755 bits/atom and 1027.056 bits/cell. These values allow us to classify juonniite as structurally very complex as well. Structural complexity parameters for cattiite, $Mg_3(PO_4)_2{\cdot}22H_2O$, which is another low-temperature hydrated phosphate associated with kampelite are 5.316 bits/atom and 419.999 bits/cell (Chernyatieva et al. 2013; structure of intermediate complexity according to Krivovichev (2013)). The formation of kampelite (1244.304 bits/cell), junnoiite (1027.056 bits/cell), and cattiite (419.999 bits/cell) due to the alteration of primary baddeleyite (19.020 bits/cell), apatite (111.419 bits/cell), and dolomite (15.710 bits/cell) demonstrates the general tendency of increasing structural and chemical complexity of minerals that form at the late low-temperature stages of hydrothermal activity (Krivovichev 2013).

Acknowledgements We are grateful to I.V. Melik-Gaikazov and V.A. Sokharev for co-operation in the geological study of the Kovdor phoscorite-carbonatite complex. Constructive comments of two anonymous reviewers and Editor-in-Chief Lutz Nasdala are gratefully acknowledged. This research was supported by the Russian Science Foundation, grant 16-17-10173.

References

Anovitz LM, Essene EJ (1987) Phase equilibria in the system $CaCO_3$-$MgCO_3$-$FeCO_3$. J Petrol 28:389–414

Blatov VA, Shevchenko AP, Proserpio DM (2014) Applied topological analysis of crystal structures with the program package ToposPro. Crystal Growth Des 14:3576–3586

Britvin SN, Ferraris G, Ivaldi G, Bogdanova AN, Chukanov NV (2002) Cattiite, $Mg_3(PO_4)_2{\cdot}22H_2O$, a new mineral from Zhelezny mine (Kovdor massif, Kola Peninsula, Russia). N Jb Miner Monat 4: 160–168

Britvin SN, Dolivo-Dobrovolsky DV, Krzhizhanovskaya MG (2017) Software for processing of X-ray powder diffraction data obtained from the curved image plate detector of Rigaku RAXIS Rapid II diffractometer. Zap Ross mineral Obsh, accepted (in Russian)

Bruker-AXS (2014) APEX2. Version 2014.11–0. Madison, Wisconsin, USA.

Chernyatieva AP, Krivovichev SV, Britvin SN (2013) The crystal structure of cattiite, $Mg_3(PO_4)_2{\cdot}22H_2O$. Zap Ross Mineral Obsh 142(2): 120–128 (in Russian)

Frost RL, Weier ML, Williams PA, Leverett P, Kloprogge JT (2007) Raman spectroscopy of the sampleite group of minerals. J Raman Spectrosc 38:574–583

Frost RL, Xi Y, Scholz R, Lopez A, Belotti FM (2013) Vibrational spectroscopic characterization of the phosphate mineral hureaulite – $(Mn, Fe)_5(PO_4)_2(HPO_4)_2{\cdot}4(H_2O)$. Vib Spectrosc 66:69–75

Ghiorso MS, Evans BW (2008) Thermodynamics of rhombohedral oxide solid solutions and a revision of the Fe-Ti two-oxide geothermometer and oxygen-barometer. Amer J Sci 308:957–1039

Huminicki DMC, Hawthorne FC (2002) The crystal chemistry of phosphate minerals. In. Kohn ML, Rakovan J, Hughes JM (eds) Phosphates. Rev Mineral Geochem, vol 48. Mineral Soc Am, Chantilly, pp 123–254

Ivanyuk GY, Yakovenchuk VN, Pakhomovsky YA (2002) Kovdor. Laplandia Minerals, Apatity, p 326

Ivanyuk GY, Kalashnikov AO, Pakhomovsky YA, Mikhailova JA, Yakovenchuk VN, Konopleva NG, Sokharev VA, Bazai AV, Goryainov PM (2016) Economic minerals of the Kovdor baddeleyite-apatite-magnetite deposit, Russia: mineralogy, spatial distribution, and ore processing optimization. Ore Geol Rev 77: 279–311

Kalashnikov AO, Yakovenchuk VN, Pakhomovsky YA, Bazai AV, Sokharev VA, Konopleva NG, Mikhailova JA, Goryainov PM, Ivanyuk GY (2016) Scandium of the Kovdor baddeleyite–apatite–magnetite deposit (Murmansk region, Russia): mineralogy, spatial distribution, and potential resource. Ore Geol Rev 72:532–537

Kampel' FB, Minin SE, Red'kin GM (1982) Normalizing of losing and fouling of complex ores of the Kovdor deposit. Gorny Zhurnal 7: 12–13 (in Russian)

Kampel' FB, Novozhilova VV, Bogdanovich VV, Sidorenkov AP, Popovich VF (1997) Development of the technology of apatite and baddeleyite concentrate processing by the Kovdor GOK. Gorny Zhurnal 12:21–25 (in Russian)

Krivovichev SV, Armbruster T, Yakovenchuk VN, Pakhomovsky YA, Men'shikov YP (2003) Crystal structures of lamprophyllite-2M and lamprophyllite-2O from the Lovozero alkaline massif, Kola peninsula, Russia. Eur J Mineral 15:711–718

Krivovichev SV (2012) Topological complexity of crystal structures: quantitative approach. Acta Crystallogr A 68:393–398

Krivovichev SV (2013) Structural complexity of minerals: information storage and processing in the mineral world. Mineral Mag 77:275–326

Krivovichev SV (2014) Which inorganic structures are the most complex? Angew Chem Int Ed 53:654–661

Liferovich RP, Yakovenchuk VN, Pakhomovsky YA, Bogdanova AN, Britvin SN (1997) Juonniite, a new mineral of scandium from calcite-dolomite carbonatites of the Kovdor massif. Zap Ross Mineral Obsh 126:56–63 (in Russian)

Lokshin EP, Lebedev VN, Lyakhov VP, Kampel' FB, Popovich V (2002) Production of zirconium-bearing ceramic and refractory matherials from the baddeleyite concentrate of the Kovdor GOK. Ogneupory i Tekhnicheskaya Keramica 11:34–40 (in Russian)

Lyakhov VP, Kampel' FB, Bogdanovich VV (1997) Complex using of mineral resources at the Kovdor GOK in new economic situation. Gorny Zhurnal 12:8–11 (in Russian)

Mandarino JA (1981) The Gladstone–dale relationship: part IV. The compatibility concept and its application. Can Mineral 19:441–450

Menezes PW, Hoffmann S, Yu P, Kniep R (2008) Crystal structure of dilithium scandium (monophosphatemonohydrogenmonophosphate), $Li_2Sc[(PO_4)(HPO_4)]$. Z Kristallogr New Cryst Str 223:319–320

Menezes PW, Hoffmann S, Yu P, Kniep R (2009) Synthesis and crystal structures of $KSc(HPO_4)_2$. Z Anorg Allg Chem 635:33–35

Mikhailova JA, Kalashnikov AO, Sokharev VA, Pakhomovsky YA, Konopleva NG, Yakovenchuk VN, Bazai AV, Goryainov PM, Ivanyuk GY (2016) 3D mineralogical mapping of the Kovdor phoscorite–carbonatite complex (Russia). Miner Dep 51:131–149

Moore PB (1974) I. Jahnsite, segelerite, and robertsite, three new transition metal phosphate species. II. Redefinition of overite, an isotype of segelerite. III. Isotypy of robertsite, mitridatite, and arseniosiderite. Am Mineral 59:48–59

Moore PB, Araki T (1977) Overite, segelerite, and jahnsite: a study in combinatorial polymorphism. Am Mineral 62:692–702

Pankova YA, Gorelova LA, Krivovichev SV, Pekov IV (2017) The crystal structure of ginorite, $Ca_2[B_{14}O_{20}(OH)_6](H_2O)_5$, and the analysis of dimensional reduction and structural complexity in the CaO-B_2O_3-H_2O system. Eur J Mineral, accepted

Rodionov NV, Belyatsky BV, Antonov AV, Kapitonov IN, Sergeev SA (2012) Comparative in-situ U–Th–Pb geochronology and trace element composition of baddeleyite and low-U zircon from carbonatites of the Palaeozoic Kovdor alkaline–ultramafic complex, Kola Peninsula, Russia. Gondwana Res 21:728–744

Sheldrick GM (2008) A short history of SHELX. Acta Crystallogr A64: 112–122

Yakovenchuk VN, Ivanyuk GY, Mikhailova JA, Selivanova EA, Krivovichev SV (2006) Pakhomovskyite, the co-dominant analogue of vivianite, a new mineral species from Kovdor, Kola Peninsula, Russia. Can Mineral 44:117–123

Yang H, Li C, Jenkins RA, Downs RT, Costin G (2007) Kolbeckite, $ScPO_4{\cdot}2H_2O$, isomorphous with metavariscite. Acta Crystallogr C 63:91–92